Nonadiabatic Dynamics of Two Strongly Coupled Nanomechanical Resonator Modes

Thomas Faust, Johannes Rieger, Maximilian J. Seitner, Peter Krenn, Jörg P. Kotthaus,* and Eva M. Weig†

Center for NanoScience (CeNS) and Fakultät für Physik, Ludwig-Maximilians-Universität, Geschwister-Scholl-Platz 1, München 80539, Germany

(Received 19 January 2012; published 17 July 2012)

The Landau-Zener transition is a fundamental concept for dynamical quantum systems and has been studied in numerous fields of physics. Here, we present a classical mechanical model system exhibiting analogous behavior using two inversely tunable, strongly coupled modes of the same nanomechanical beam resonator. In the adiabatic limit, the anticrossing between the two modes is observed and the coupling strength extracted. Sweeping an initialized mode across the coupling region allows mapping of the progression from diabatic to adiabatic transitions as a function of the sweep rate.

DOI: 10.1103/PhysRevLett.109.037205 PACS numbers: 85.85.+j, 05.45.Xt, 62.25.Fg

The time dynamics of two strongly coupled harmonic oscillators follows the Landau-Zener model [1–4], which is used to describe the quantum mechanical mode tunneling in a nonadiabatic transition. This phenomenon is observed and utilized in many areas of physics, e.g., atomic resonances [5], quantum dots [6], superconducting qubits [7], and nitrogen-vacancy centers in diamond [8]. It is also possible to create classical model systems exhibiting the same time evolution, which until now have been restricted to optical configurations [9,10]. Such systems are well suited for the study of diabatic behavior over a wide parameter space; for example, nonlinearities could be readily introduced, potentially leading to chaotic behavior [9,11].

Nanomechanical resonators with frequencies in the MHz range can be realized with high mechanical quality factors [12,13] and easily tuned [14] in frequency. This makes them particularly well suited for exploration of their coupling to other mechanical, optical, or electrical microwave resonators. Strong cavity coupling in the optical or microwave regime has been widely studied as it enables both cooling and self-oscillation of the mechanical modes [15–18]. In addition, the time-resolved Rabi oscillations between a strongly coupled two-level system and a micromechanical resonator have been observed [19].

Purely mechanical, static coupling between different resonators [20–23] and between different harmonic modes of the same resonator [24] has also been demonstrated. Here, we explore the coupling between the two fundamental flexural modes [25] of a single nanomechanical beam vibrating in plane and out of plane, respectively. We study the adiabatic to nonadiabatic transitions between the two strongly coupled classical mechanical modes in time-dependent experiments, in correspondence to the Landau-Zener transition.

The nanomechanical high-stress silicon nitride string used in this work is shown in Fig. 1. Two parallel gold electrodes vertically offset to the beam are used to dielectrically couple the beam oscillation to an external microwave cavity with a quality factor of ≈ 70 at a resonance frequency of 3.44 GHz [26]. Displacement of the resonator leads to a change in capacitance between the two electrodes, thereby detuning the resonance frequency of the microwave circuit and creating sidebands with a frequency offset equal to the mechanical eigenfrequency. The inductively coupled microwave cavity is driven by a signal generator; the transmission signal is demodulated and fed to a spectrum analyzer as depicted in Fig. 1 and described in more detail in [26]. In addition, a microwave bypass capacitor is used in the ground connection of one electrode which allows application of additional dc bias and rf voltages to the electrodes. This is used to actuate the mechanical resonator via the dielectric driving mechanism [14,27]. At the same time, the dielectric coupling

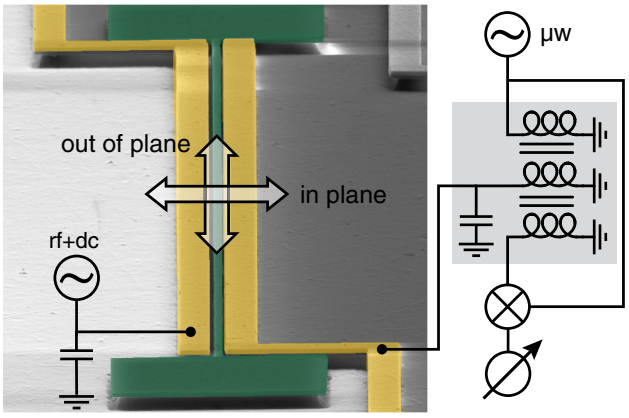

FIG. 1 (color online). The SEM micrograph of the 55 μm long and 260-nm wide silicon nitride string resonator [green (dark gray)] taken at an angle of 85° also depicts the two adjacent gold electrodes [yellow (light gray)] used to dielectrically drive, tune, and read out the resonator motion. The arrows denote the two mechanical modes, one oscillating parallel and the other perpendicular to the plane of the chip. The simplified measurement scheme [26] shows the connection of the electrodes to the readout cavity (gray box) and the microwave bypass capacitor in the bottom left.

provides a way to tune the resonance frequency of the two mechanical modes: The static electric field between the electrodes polarizes the dielectric resonator material which is then attracted to high electric fields, thereby changing the spring constant of the modes via the resulting force gradient [14]. In the chosen geometry, where the bottom of the electrodes is flushed with the top of the beam [26], a rising dc bias voltage causes the frequency of the in-plane mode to decrease and the out-of-plane frequency to increase [28]. All experiments are performed at room temperature at pressures below 5×10^{-4} mbar.

At low dc bias voltages, the in-plane mode of the 55 μm long beam has a higher resonance frequency than the out-of-plane mode. This is a result of the 260 nm beam width exceeding the beam's thickness of 100 nm, which leads to a higher rigidity for the in-plane mode [13]. Thus, by increasing the dc bias voltage, we are able to tune the two modes into resonance at a common frequency of approximately 6.63 MHz. The coupling between the modes has been observed for several resonators on various chips and is at least partially caused by the spatially inhomogeneous electric field [29]. There might also be an additional, purely mechanical coupling mediated by the prestress in the beam. The characteristic avoided crossing diagram of two coupled oscillators can be obtained by measuring the driven response of the two modes at different dc bias voltages, as shown in Fig. 2.

Splitting this diagram into an upper and lower branch and fitting each data set with a Lorentzian allows the extraction of the resonance frequencies and quality factors for each dc bias voltage applied to the electrodes. Both modes exhibit a quality factor of approximately 80 000, somewhat lower than in previous measurements [26], presumably caused by fabrication imperfections. The eigenfrequencies extracted from the anticrossing diagram are depicted in Fig. 3. A few data points around 6.5 and 7.4 V in the upper branch were omitted because of an insufficient signal to noise ratio.

For our system, the standard model of two coupled harmonic oscillators [30] needs to be expanded, as both oscillators react differently to the tuning parameter (the dc bias voltage). We use the generalized differential equation for the displacement u_n of each mode n ($n = 1, 2$)

$$m_{\mathrm{eff}} u_n'' + m_{\mathrm{eff}} \gamma u_n' + k_{nm} u_n = 0 \tag{1}$$

with

$$k_{nm} = \begin{pmatrix} k_1 + k_c & -k_c \\ -k_c & k_2 + k_c \end{pmatrix}, \tag{2}$$

where m_{eff} denotes the effective mass and $\gamma = \omega/Q$ the damping constant of the resonator (identical for both modes), k_c the coupling between the two modes, and k_n the spring constant of the respective mode. As the dc bias voltage polarizes the resonator material and creates an electric field gradient, the additional force gradient seen by the beam depends on the square of the voltage. We use a second-order series expansion around U_0 to describe the tuning behavior: $k_n = k_0 + \kappa_n(U - U_0) + \lambda_n(U - U_0)^2$ with κ_n and λ_n as linear and quadratic tuning constants, assuming that both modes have the same spring constant k_0 at the voltage U_0 corresponding to zero detuning. Note that the influence of the quadratic term is less than 15% in the whole voltage range [29]. The two solutions of the differential equation (1) describe the two branches, and their fit to the experimental data is shown as solid lines in Fig. 3. The extracted frequency splitting

$$\frac{\Gamma}{2\pi} = \frac{1}{2\pi}\left(\sqrt{\frac{k_0 + 2k_c}{m_{\mathrm{eff}}}} - \sqrt{\frac{k_0}{m_{\mathrm{eff}}}}\right) = 7.77\ \mathrm{kHz} \tag{3}$$

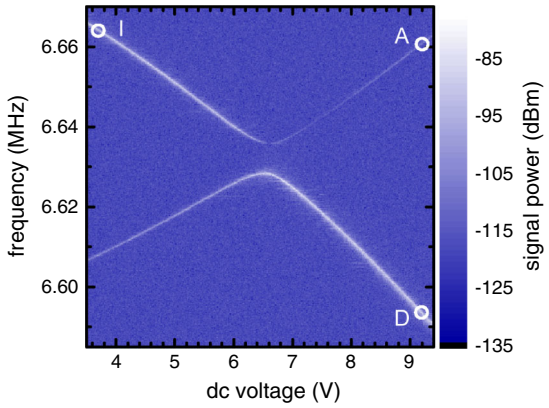

FIG. 2 (color online). Both mechanical modes can be tuned in opposite direction by increasing the dc bias voltage applied to the electrodes. The signal power of the driven resonances is shown color-coded versus dc voltage and drive frequency. Note the clear avoided crossing between the two modes. The three circles denote the initial state (I) and two possible final states after an adiabatic (A) or diabatic (D) transition through the coupling region, as described in the text.

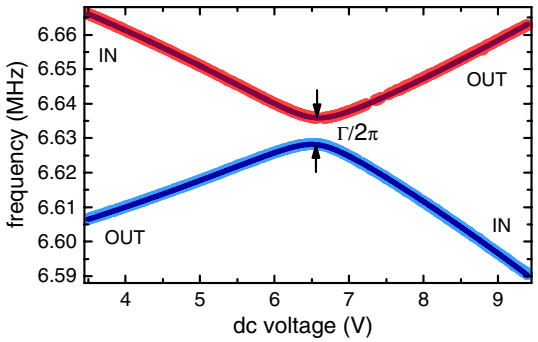

FIG. 3 (color online). Frequency of the upper (red) and lower (blue) branch versus dc bias voltage. Each dot represents a value extracted from a Lorentzian fit of the data shown in Fig. 2, and the solid lines are a fit of the theoretical model described in the text. IN and OUT denote the in- and out-of-plane mode of the beam.

at $U_0 = 6.547$ V is much larger than the linewidth of $\gamma/2\pi = 82$ Hz; thus, the system is clearly in the strong-coupling regime.

When slowly (adiabatically) tuning the system through the coupling region, the system energy will remain in the branch in which it was initialized, thereby transforming an out-of-plane oscillation to an in-plane motion (and vice-versa for the other mode). At high tuning speeds, the diabatic behavior dominates and there is no mixing between the modes. This classical behavior [30] is analogous to the well-known quantum mechanical Landau-Zener transition. The transition probabilities are identical in the quantum and classical case:

$$P_{\mathrm{dia}} = \exp\left(-\frac{\pi\Gamma^2}{2\alpha}\right), \qquad P_{\mathrm{adia}} = 1 - P_{\mathrm{dia}}, \tag{4}$$

where the change of the frequency difference between the two modes in time

$$\alpha = \frac{\partial(\omega_1 - \omega_2)}{\partial t} \quad \text{using } \omega_n = \sqrt{\frac{k_n}{m_{\mathrm{eff}}}} \tag{5}$$

denotes the tuning speed [29].

The measurement sequence is depicted in Fig. 4(a): the system is initialized at point I (see Fig. 2) by applying a 6.6647 MHz tone and a dc bias voltage of 3.6 V to the electrodes. At $t = 0$, the voltage (blue line) is now ramped up to 9.1 V within time τ. As the start and stop frequencies are kept constant throughout the experiment, changing τ changes the tuning speed α and, therefore, the transition probability. Thus, the system's energy is distributed between point A or D (see Fig. 2), depending on the ramp time τ. At $t = 0$, the mechanical resonator gets detuned from the constant drive frequency. Therefore, its energy starts to decay as reflected by the decreasing signal power [green dashed line in Fig. 4(a)]. After a short additional delay of δ (to avoid transient artifacts in the measurement), the decay of the mechanical oscillation is recorded with the spectrum analyzer. An exponential fit to the signal power, symbolized by the dotted black line in Fig. 4(a) allows the extraction of the oscillation magnitude at $t = \tau$, which is normalized to the magnitude measured before the transition at point I to account for slight variations in the initialization. This experiment is repeated with many different ramp times τ and with the detection frequency of the spectrum analyzer set to monitor either point A or D. The results of these measurements are shown in Fig. 4(b). The data clearly show the expected behavior: For short ramp times below 0.2 ms, the diabatic behavior dominates. For long ramp times, the adiabatic transition prevails, even though mechanical damping decreases the signal for large τ.

As can be seen in the inset of Fig. 4(b), the sum of the two curves perfectly follows the exponential decay of the mechanical energy (solid line). This decay in amplitude between $t = 0$ and $t = \tau$ has to be accounted for in the theoretical model and, therefore, an additional decay term $e^{-\gamma t}$ is introduced to Eqs. (4). The solid lines in Fig. 4(b) show the resulting transition probabilities to point A and D and are calculated by using the α and Γ obtained from the data in Fig. 3. The measured data was rescaled by a constant factor with no free parameters to represent the probability distribution of the resonator's energy after a transition [29]. A third state, representing the probability that the mechanical energy decays, is required to keep the sum of the probabilities at one. It is determined from the inset and shown as a green dashed line in Fig. 4(b). The corresponding decay constant $1/\gamma = 1.92$ ms is identical to the one extracted from the spectrally measured quality factor. Note that dynamics with a time constant much smaller than $1/\gamma$ are observed, demonstrating coherent control of the system.

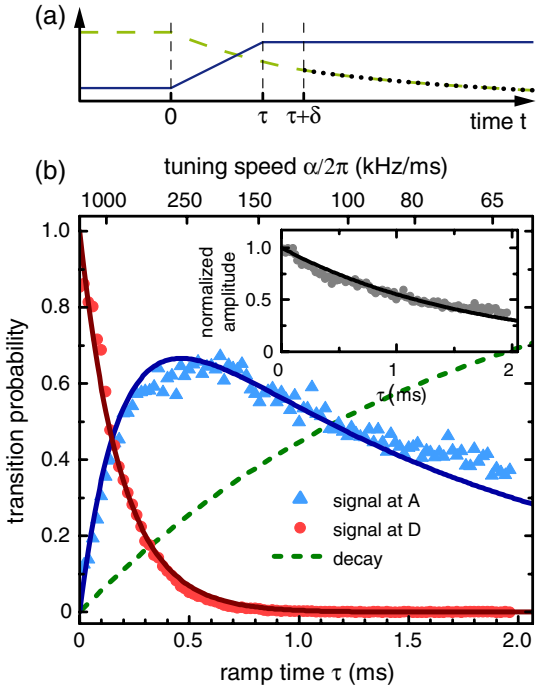

FIG. 4 (color online). The measurement sequence of the time-resolved experiment is shown in (a). At $t = 0$, the dc bias voltage (blue line) is ramped up in the timespan τ, after the delay δ the measurement of the mechanical signal power (green dashed line) starts at point A or D in Fig. 2 and a fit (black dotted line) is used to extract the magnitude of the beam oscillation at $t = \tau$. The normalized signal power at $t = \tau$ and, thus, the transition probability obtained for different ramp times τ measured at point A in Fig. 2 (blue triangles) or point D (red dots) is plotted in (b) together with the theoretical model described in the text (solid lines). The inset shows the sum of both measurements and displays a clear exponential decay. The corresponding decay probability is represented by a green dashed line in the main plot.

In conclusion, we utilize the strong coupling between two orthogonal modes of the same nanomechanical resonator by tuning these two modes into resonance to analyze their time-dependent dynamics. After characterizing the coupling, we are able to model the time-resolved transition

behavior between the two modes. The entire dynamic range between fast and coherent diabatic and slow adiabatic passages is accessible in the experiment, and a good agreement between theory and experiment is observed.

The experiment is conducted with approximately 10^9 phonons in the vibrational mode of the resonator; thus, not the single-particle probability function but the energy distribution of the ensemble is measured in the classical limit. Since the (strongly) nonlinear regime of the utilized nanomechanical resonator can be easily accessed, the presented system could also be used to study the coupling and the time-dependent transitions of two nonlinear oscillators [31,32] and the development of chaotic behavior [11,32] in the classical regime. Combining cavity-pumped self-oscillation [16] with the coupled resonator modes presented here allows the study of synchronization and collective dynamics in nanomechanical systems, as theoretically predicted [33,34]. Furthermore, after the recent breakthrough in the ground state cooling of mechanical resonators [17–19], the coupling between two quantum mechanical elements becomes accessible.

Financial support by the Deutsche Forschungsgemeinschaft via Project No. Ko 416/18, the German Excellence Initiative via the Nanosystems Initiative Munich (NIM) and LMUexcellent, as well as the European Commission under the FET-Open project QNEMS (233992) is gratefully acknowledged. We thank Andreas Isacsson for stimulating discussions and Darren R. Southworth for critically reading the manuscript.

*kotthaus@lmu.de
†weig@lmu.de

[1] L. D. Landau, Phys. Z. Sowjetunion **2**, 46 (1932).
[2] C. Zener, Proc. R. Soc. A **137**, 696 (1932).
[3] E. C. G. Stueckelberg, Helv. Phys. Acta **5**, 369 (1932).
[4] E. Majorana, Nuovo Cimento **9**, 43 (1932).
[5] J. R. Rubbmark, M. M. Kash, M. G. Littman, and D. Kleppner, Phys. Rev. A **23**, 3107 (1981).
[6] J. R. Petta, H. Lu, and A. C. Gossard, Science **327**, 669 (2010).
[7] M. Sillanpää, T. Lehtinen, A. Paila, Y. Makhlin, and P. Hakonen, Phys. Rev. Lett. **96**, 187002 (2006).
[8] G. D. Fuchs, G. Burkard, P. V. Klimov, and D. D. Awschalom, Nature Phys. **7**, 789 (2011).
[9] R. J. C. Spreeuw, N. J. van Druten, M. W. Beijersbergen, E. R. Eliel, and J. P. Woerdman, Phys. Rev. Lett. **65**, 2642 (1990).
[10] D. Bouwmeester, N. H. Dekker, F. E. V. Dorsselaer, C. A. Schrama, P. M. Visser, and J. P. Woerdman, Phys. Rev. A **51**, 646 (1995).
[11] J. Kozłowski, U. Parlitz, and W. Lauterborn, Phys. Rev. E **51**, 1861 (1995).
[12] S. S. Verbridge, J. M. Parpia, R. B. Reichenbach, L. M. Bellan, and H. G. Craighead, J. Appl. Phys. **99**, 124304 (2006).
[13] Q. P. Unterreithmeier, T. Faust, and J. P. Kotthaus, Phys. Rev. Lett. **105**, 027205 (2010).
[14] Q. P. Unterreithmeier, E. M. Weig, and J. P. Kotthaus, Nature (London) **458**, 1001 (2009).
[15] S. Gröblacher, K. Hammerer, M. R. Vanner, and M. Aspelmeyer, Nature (London) **460**, 724 (2009).
[16] E. Verhagen, S. Deléglise, S. Weis, A. Schliesser, and T. J. Kippenberg, Nature (London) **482**, 63 (2012).
[17] J. D. Teufel, T. Donner, D. Li, J. W. Harlow, M. S. Allman, K. Cicak, A. J. Sirois, J. D. Whittaker, K. W. Lehnert, and R. W. Simmonds, Nature (London) **475**, 359 (2011).
[18] J. Chan, T. P. Mayer Alegre, A. H. Safavi-Naeini, J. T. Hill, A. Krause, S. Gröblacher, M. Aspelmeyer, and O. Painter, Nature (London) **478**, 89 (2011).
[19] A. D. O'Connell, M. Hofheinz, M. Ansmann, R. C. Bialczak, M. Lenander, E. Lucero, M. Neeley, D. Sank, H. Wang, M. Weides, J. Wenner, J. M. Martinis, and A. N. Cleland, Nature (London) **464**, 697 (2010).
[20] H. Okamoto, T. Kamada, K. Onomitsu, I. Mahboob, and H. Yamaguchi, Appl. Phys. Express **2**, 062202 (2009).
[21] R. B. Karabalin, M. C. Cross, and M. L. Roukes, Phys. Rev. B **79**, 165309 (2009).
[22] R. B. Karabalin, R. Lifshitz, M. C. Cross, M. H. Matheny, S. C. Masmanidis, and M. L. Roukes, Phys. Rev. Lett. **106**, 094102 (2011).
[23] S. Perisanu, T. Barois, P. Poncharal, T. Gaillard, A. Ayari, S. T. Purcell, and P. Vincent, Appl. Phys. Lett. **98**, 063110 (2011).
[24] H. J. R. Westra, M. Poot, H. S. J. van der Zant, and W. J. Venstra, Phys. Rev. Lett. **105**, 117205 (2010).
[25] I. Kozinsky, H. W. Ch. Postma, I. Bargatin, and M. L. Roukes, Appl. Phys. Lett. **88**, 253101 (2006).
[26] T. Faust, P. Krenn, S. Manus, J. P. Kotthaus, and E. M. Weig, Nature Commun. **3**, 728 (2012).
[27] S. Schmid, M. Wendlandt, D. Junker, and C. Hierold, Appl. Phys. Lett. **89**, 163506 (2006).
[28] J. Rieger, T. Faust, M. J. Seitner, J. P. Kotthaus, and E. M. Weig, arXiv:1207.2403.
[29] See Supplemental Material at http://link.aps.org/supplemental/10.1103/PhysRevLett.109.037205 for the solution of the coupled differential equations, details of the tuning behavior, the data analysis, and the coupling mechanism.
[30] L. Novotny, Am. J. Phys. **78**, 1199 (2010).
[31] J. Liu, L. Fu, B.-Y. Ou, S.-G. Chen, D.-I. Choi, B. Wu, and Q. Niu, Phys. Rev. A **66**, 023404 (2002).
[32] Q. Zhang, P. Hänggi, and J. Gong, New J. Phys. **10**, 073008 (2008).
[33] G. Heinrich, M. Ludwig, J. Qian, B. Kubala, and F. Marquardt, Phys. Rev. Lett. **107**, 043603 (2011).
[34] R. Lifshitz, E. Kenig, and M. C. Cross, in *Fluctuating Nonlinear Oscillators*, edited by M. T. Dykman (Oxford University Press, Oxford, to be published).